



PERGAMON

Solid State Communications 116 (2000) 287–292

solid
state
communications

www.elsevier.com/locate/ssc

Cluster-assembled carbon films with different nanostructures: a spectroscopic study

E. Riedo^a, E. Magnano^b, S. Rubini^b, M. Sancrotti^{c,*}, E. Barborini^d, P. Piseri^d, P. Milani^d

^a*Dipartimento di Fisica, Università di Milano, Via Celoria 16, I-20133 Milan, Italy*

^b*Laboratorio Nazionale TASC–INFN, Strada Statale 14, km 163.5 Basovizza, I-34012 Trieste, Italy*

^c*INFN and Dipartimento di Matematica e Fisica, Università Cattolica del Sacro Cuore, Campus of Brescia,
Via dei Musei, I-25121 Brescia, Italy*

^d*INFN–Dipartimento di Fisica, Università di Milano I, Via Celoria 16, I-20133 Milan, Italy*

Received 20 June 2000; received in revised form 22 June 2000; accepted 25 June 2000 by E. Molinari

Abstract

Carbon thin films with different nanostructures grown by Cluster Beam Deposition are studied by means of Raman Spectroscopy, X-ray photoemission spectroscopy (XPS), and electron energy loss spectroscopy (EELS). Raman and EELS of the as-grown specimens show a correlation between the properties of the free carbon clusters and the properties of the films obtained by deposition of different sized clusters. In contrast, the inhomogeneous character of the films is not reflected in the valence band states as seen by XPS. © 2000 Elsevier Science Ltd. All rights reserved.

Keywords: A. Thin films; A. Nanostructures; D. Electronic states; E. Photoelectron spectroscopies; E. Electron energy loss spectroscopy

PACS: 71.24.+q

1. Introduction

The use of carbon clusters and nanotubes for the synthesis of nanostructured and composite materials has been recently suggested as a means to obtain materials with novel electronic and structural properties [1–3]. Among different synthetic routes presently under development, low energy cluster beam deposition (LECBD) is gaining increasing interest as one of the most promising techniques for the synthesis of nanostructured thin films [4–6]. With LE CBD it is, in principle, possible to control the mean coordination of carbon atoms in the film and its porosity on a nano- and meso-scale which results from cluster stacking with reduced fragmentation [7]. The cluster-assembled films show novel structural and functional properties compared to carbon films assembled atom-by-atom [1,3,8].

Recently it has been shown that cluster-assembled carbon films with different nanostructures can be deposited by use of aerodynamical separation effects typical of supersonic

beams [5]. These effects consist of an enrichment of heavy clusters in the central portion of the beam and of light clusters in the peripheral one. Using supersonic beams we have deposited films characterized by regions containing clusters of different sizes, ranging from few tens of atoms per cluster up to several thousands. These different regions have different types of bonding and structures on the nanoscale.

To obtain information on how the nanostructure influences the electronic properties of these materials we report on a study of different sized samples by means of X-ray photoemission spectroscopy (XPS), electron energy loss spectroscopy (EELS), and Raman spectroscopy. In this paper we show the correlation between the properties of free precursor carbon clusters and the properties of thin films obtained by deposition of different sized clusters, and we show how EELS and XPS are sensitive to different film nanostructures.

2. Experimental

Nanostructured (NS) carbon thin films are produced by

* Corresponding author. Tel.: +39-40-3756-435; fax: +39-40-226767.

E-mail address: sancrotti@sci.area.trieste.it (M. Sancrotti).

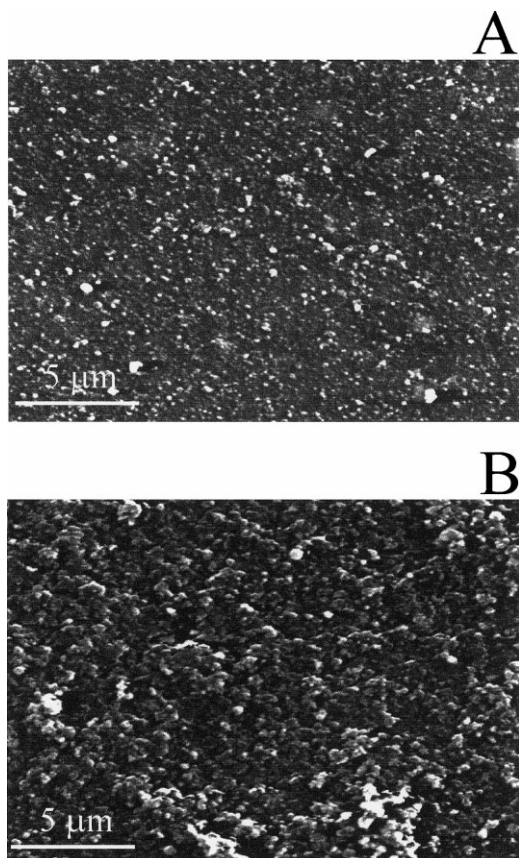


Fig. 1. Scanning electron micrographs of a typical nanostructured film: (a) region deposited with a portion of the supersonic beam rich of small clusters (RSC); (b) region deposited with a portion of the supersonic beam rich of large clusters (RLC).

deposition of supersonic cluster beams. A detailed description of the apparatus based on a pulsed microplasma cluster source (PMCS) is reported elsewhere [5,9]. Here we briefly report the operation principle: a graphite target is eroded by a pulsed microplasma produced in the cluster source. The ablated species are mixed with a pulse of helium to favor cluster condensation, the cluster–helium mixture then expands through the source nozzle into the vacuum forming a seeded supersonic beam.

Cluster mass distribution is log-normal peaked around 500 atoms per cluster. During the supersonic expansion, species with different weights are separated in the beam: in particular, large clusters are concentrated in the beam center whereas the small ones are diverted to the periphery. Films with different nanostructures can be grown by simply intersecting with a substrate different regions of the cluster beam [5]. Since the kinetic energy per atom is about 0.5 eV, the deposition of the clusters on a substrate takes place without significant fragmentation at the impact. As a consequence, the structure of carbon films is reminiscent, on

different length scales, of the precursor clusters. The deposited NS films have regions with different coordinations and local order: in particular, one end is rich of large clusters (RLC region) whereas the opposite end is rich of small clusters (RSC). In Fig. 1 we report the scanning electron microscope micrographs of two typical regions (RLC and RSC) of a film deposited on silicon. The density of the films is lower than that of other forms of carbon and depends on the type of precursor clusters: in general, large clusters have tendency to form open structures whereas small clusters form more compact films [7]. Densities ranging from ~ 1 to ~ 1.4 g/cm³ for RLC and RSC, respectively, have been found by X-ray reflectivity and Brillouin scattering [8]. The morphology of the films is characterized by a granular structure with grains with diameters of tens of nanometer.

Unpolarized Raman spectra were recorded ex situ, at room temperature in backscattering geometry, using an I.S.A. Jobin-Yvon triple-grating spectrometer with a liquid nitrogen cooled camera detection (CCD) system. The spectral resolution was about 3 cm⁻¹; the 514.5 nm line of an Ar ion laser was used as excitation source; the power on the sample was about 3 mW.

The valence-band photoemission spectra and EELS spectra were measured in a UHV chamber at the base pressure of 1×10^{-10} mbar. A conventional Mg-anode ($h\nu = 1253.6$ eV) X-ray source was used for XPS while EELS spectra were excited with an electron gun, coaxial to the electron analyzer, operating at a fixed primary beam energy of 0.7 keV. EELS data refer to the energy loss region typical of plasmons excitation. The typical maximum count rates were 100,000 counts/s for the elastic peak and 20,000 counts/s for the plasmon loss features. Charging effects were not observed on the samples during measurements.

Electrons were energy analyzed using a double-pass cylindrical mirror analyzer (CMA) operating in the retarding mode. The resulting overall energy resolution, including the excitation source and CMA, amounted to ≈ 1.1 eV for XPS and ≈ 1 eV for EELS. XPS measurements were also performed in a different UHV chamber by using a monochromatized Al-anode source ($h\nu = 1486.6$ eV) and an electrostatic hemispherical analyzer (EHA). This allowed us to work with a higher lateral spatial resolution on the samples. The typical size of the specimen area sampled via XPS and EELS is 8 mm² (CMA), 0.3 mm² (EHA), and 1 mm² (EELS). The XPS valence band spectra acquired with different lateral resolution (CMA vs. EHA) gave similar results with no significant differences regardless of the specific area sampled from the specimen. This is not the case of the EELS measurements, which actually reflect inhomogeneities in the spatial cluster distribution.

A highly oriented pyrolytic graphite (HOPG) sample freshly cleaved and a polycrystalline diamond film grown by plasma assisted chemical vapor deposition were used as reference for our measurements.

The C 1s binding energy (BE) of HOPG was set at

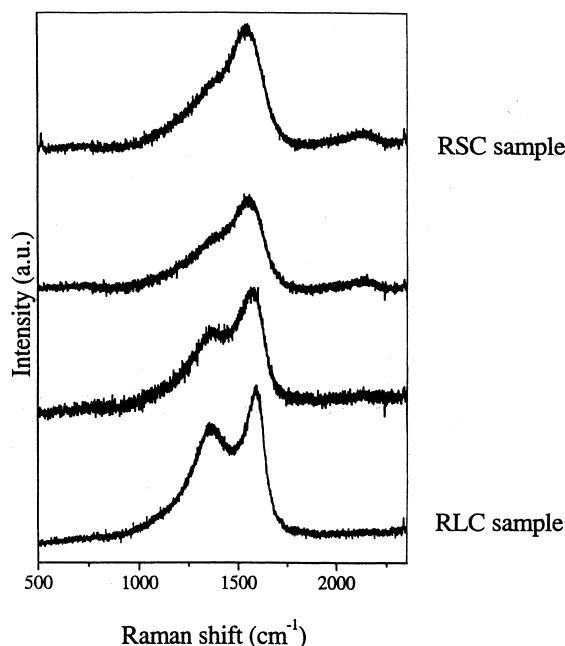


Fig. 2. First-order Raman spectra of films deposited with different portions of the cluster beam. Going from the bottom (internal part of the beam, i.e. RLC region) to the top spectrum (external part of the beam, i.e. RSC region) one can see the evolution from a disordered

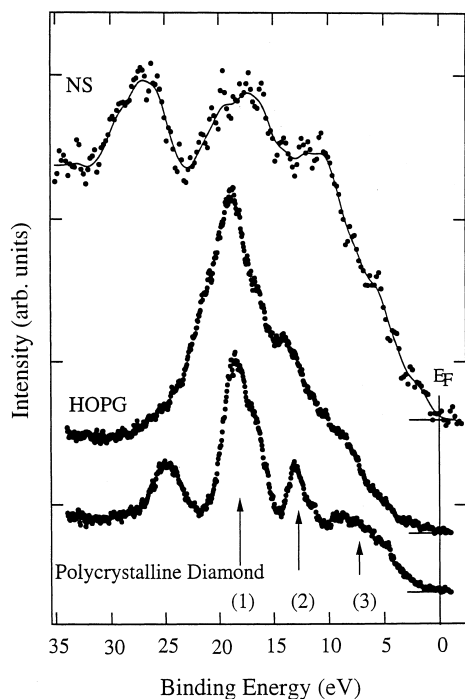


Fig. 3. XPS valence bands spectra of HOPG, diamond, and the nanostructured sample. The solid line is obtained after smoothing and it is shown as an eye-guide.

284.4 eV [10] and it was used for the calibration of the binding energy axis.

The samples, which were prepared *ex situ*, exhibit an oxygen surface contamination, resulting in a few atomic percent from the O 1s/C 1s intensity ratio, evaluated by taking into account the XPS O 1s and C 1s sensitivity factors, respectively. The complete removal of contamination was not possible because of the chemical bond changes at the surface induced by ion sputtering [11]. A signal corresponding to O 2s states is visible in the valence band photoemission spectra at ≈ 26 eV BE.

3. Results and discussion

In order to characterize the films deposited with different portions of the supersonic beam, we have performed Raman spectroscopy, which is sensitive to the carbon coordination and degree of crystallinity on a nanometric scale (Fig. 2). The top spectrum in Fig. 2 is taken on a RSC region (periphery of the beam). The shape and the shift of the peak (G band) are typical of a highly disordered carbon [12]. The D peak is present as a broad shoulder on the left of the G band.

Going from the top to the bottom spectrum in Fig. 2, one can follow the evolution from an amorphous towards a disordered graphitic structure by shifting from the periphery of the beam towards the central region (RLC region). This evolution is confirmed by a hardening of the G peak, the appearance of a well-defined D band, and by the narrowing of the two Raman lines. All these parameters are in agreement with a more pronounced graphitic ordering of the sample [12].

The spectra are typical of a disordered carbon with a high degree of sp^2 coordination. The spectral features relative to broadened and highly overlapping G and D bands suggest that the Phonon Density of States is different from that of graphite because of the presence of different types of disorder (bond angle and length defects, different coordination with respect to graphitic sp^2). The degree of disorder is such that, even in the RLC region, the Tuinstra–Koenig relationship is not valid [12].

The XPS valence-band (VB) spectra of polycrystalline diamond, of the HOPG sample, and of the nanostructured sample are shown in Fig. 3. Despite the structural inhomogeneities of the film, no significant changes have been observed in the VB spectra while moving from the RSC to the RLC region. For this reason we report only one spectrum representative of all the regions of the sample. In Fig. 3 each spectrum shows a broad and intense peak (1) at about 20 eV, a second peak (2) between 10 and 15 eV and a third not well-defined shoulder (3) between 10 eV and the top of the valence band. The first peak is ascribed to structures of primarily C 2s character, the second peak has a mixed sp -origin, while the structure (3) can be related to $2p_\sigma$ and $2p_\pi$ orbitals [13]. The valence band XPS spectra reflect the density of the states (DOS) as filtered by the cross-section

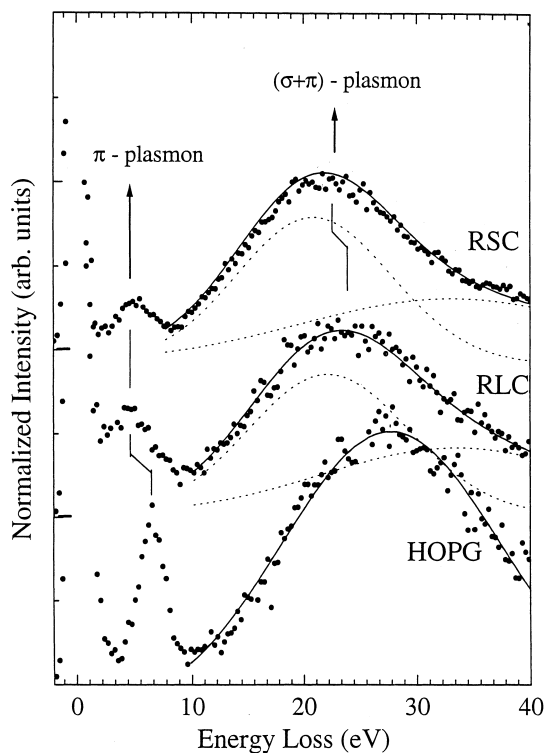


Fig. 4. EELS spectra of: (a) HOPG; (b) RLC region; (c) RSC region. The $\sigma + \pi$ peak is resolved into Gaussian components.

values that depend on the orbital symmetry as broadened by instrumental and inherent effects. The cross-section ratios for the Mg $K\alpha$ radiation are $\sigma(C\ 2s) : \sigma(C\ 2p_\sigma) : \sigma(C\ \beta 2p_\pi) = 13 : 1 : 0.5$ [13,14]. The DOS of diamond and graphite were calculated by Schäfer et al. [13] and compared with the valence band XPS spectra. As shown in Fig. 3, the peak (1) in graphite is broader than that of diamond. The peak (2) at 13 eV is sharper and higher with respect to peak (1) in diamond than in graphite. This feature arises from the L_1 maximum in the DOS of diamond compared to the Q^+1u maximum in the DOS of graphite [13]. The peak (2) at about 13 eV was detected also in the XPS valence band of polyethylene which, as diamond, presents a sp^3 hybridization [15]. In Fig. 3 the origin of the peak at 11 eV in the spectrum of the nanostructured sample is not clear and it can depend on the particular nanostructured nature of this sample. Also in the region of peak (3) the spectrum of the nanostructured sample reveals a structure with other than sp^2 character. Due to the lack of reliable theoretical models describing these nanostructured systems, no further spectral assignment is possible. Peak (3) has two components: the p_π -band peak in the energy range of 2–4 eV and the p_σ -band peak in the range of 6–9 eV [16]. Since the photoemission cross-section of the p_π -band peak is low with respect to the other contributions, this p_π -band structure is hardly visible in the XP spectra. In contrast,

the p_σ -band peak is visible as a shoulder, and it is more evident in diamond than in graphite [13].

The NS sample spectrum also shows a structure at 26 eV, which is assigned to O 2s due to contamination. On the other hand, the O 2p structure is significantly attenuated with respect to the O 2s feature due to its smaller cross-section [17]. This contamination is found to be homogeneous across the samples; thereby any difference seen while probing different portions of the specimen are to be assigned to the specific inherent film character.

Electron-energy-loss spectra of the RLC and RSC regions of the nanostructured film and the HOPG sample are shown in Fig. 4 after subtracting the contributions from double scattering and the background. It is worth observing that differently from the XPS analysis and similarly with Raman characterization, EELS reveals some important differences between RSC and RLC regions. The spectrum of HOPG shows loss features at 6.6 and 27.6 eV, representing the collective excitations of two groups of valence electrons present in the sp^2 bonded system. The former is a π plasmon due to the π electrons alone and the latter is the plasmon due to all the valence electrons [18]. The loss spectra of the RLC and RSC regions display two loss features attributed to the π and $\sigma + \pi$ plasmons. The $\sigma + \pi$ plasmon appears at 23.4 and 21.7 eV for the RLC and RSC regions, respectively. This is, in both cases, at a reduced energy as compared to HOPG. This can be due to the lower atomic density of our samples with respect to graphite. In fact the plasmon energy is predicted by the free electron model to be equal to:

$$\omega_p = \sqrt{\frac{4\pi n_e e^2}{m^*}} \quad (1)$$

where n_e is the electron density of the material and m^* and e are the electronic effective mass and charge [19]. The $\sigma + \pi$ plasmon peak position in the RLC region is at 23.4 eV, while in the RSC region it is at 21.7 eV. Consistently with the model of formula (1), these shifts in the $\sigma + \pi$ plasmon peak position indicate a progressive decrease in the density of free electrons. Since the RSC region has a density higher than RLC, the plasmon shift can be related to a decrease in the density of delocalized electrons having as a counterpart the increase of “defects” such as non-hexagonal rings [7,12]. The more “defective” structure of RSC observed by Raman spectroscopy is thus reflected also in the electronic structure.

By comparison of the portions of the EELS spectra closer to the elastic peak (Fig. 4) we note that the peak related to π -electrons decreases in intensity going from the spectrum of graphite, to the spectrum of the RLC specimen and finally to the spectrum of the RSC specimen. We note that the π -electrons of graphite have a delocalized character, thereby the decrease in intensity of the π plasmon peak observed in the nanostructured specimens reflects in turn a progressive decrease of the “graphitic” character (from graphite to RLC

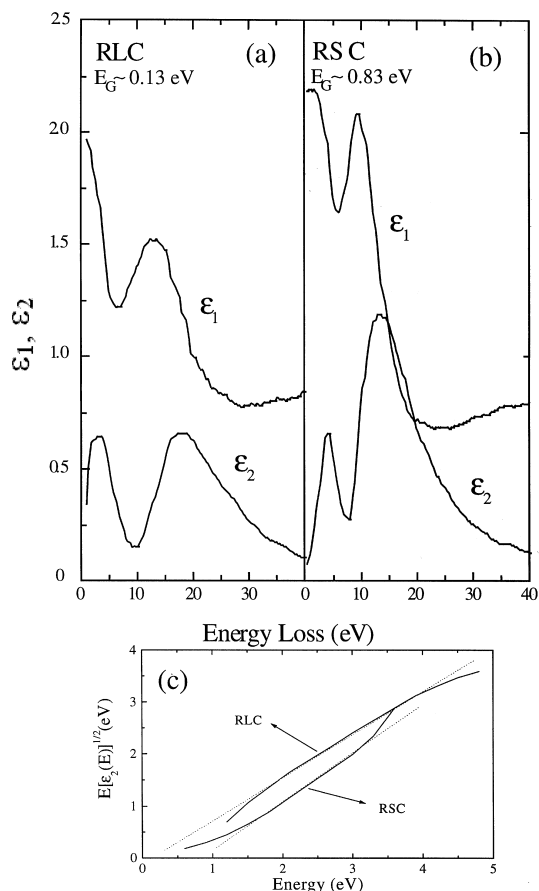


Fig. 5. Real part ϵ_1 and imaginary part ϵ_2 of the dielectric function obtained for (a) the RLC sample and (b) and for the RSC sample. Panel (c) shows the fits to the experimental data by using Tauc's formula [22].

and then to RSC). This is consistent with the analysis based on Raman spectroscopy.

The EELS spectra corrected for multiple scattering, surface losses, and instrumental broadening are proportional to $\text{Im}(-1/\epsilon(E))$. This loss function in turn can be used to generate both parts of the dielectric function using the Kramers–Kronig (KK) relationships [20]. KK analysis of the CMA-EELS spectra collected with primary beam energies of 500 eV and higher was discussed for example by Kovaric et al. [18] and Egerton [20] in the case of carbon-based systems, also including graphite. The integration with respect to energy in the analysis was carried out by extrapolating the loss function up to 150 eV using an inverse power law AE^{-r} . The constants A and r were calculated by fitting the last 10 terms of the loss spectra [20]. For graphite we obtain the functions $\epsilon_1(E)$, $\epsilon_2(E)$ (real and imaginary part of the dielectric function) which are not shown for space limitations. Taft and Philipp [21] have found, with optical measurements, π – π^* transitions at ≈ 4 eV and σ – σ^* transitions at ≈ 12 eV.

$\epsilon_1(E)$ and $\epsilon_2(E)$ of the nanostructured carbon samples in the RLC and RSC regions are shown in Fig. 5. The maximum of $\epsilon_2(E)$ related to π – π^* transitions is located at ≈ 3.6 eV in the RLC region and at ≈ 4.2 eV in the RSC region. There is a second large structure in the two spectra with maxima at ≈ 18 and ≈ 13.5 eV for the RLC and RSC regions, respectively. These peaks correspond to π – σ^* , σ – π^* , σ – σ^* transitions.

The NS carbon band gap can be extracted from the relationship

$$E^2 \epsilon_2(E) = k(E - E_{\text{BG}})^2 \quad (2)$$

where E_{BG} represents the band gap and k is a constant specific of the sample. This relationship has been reported by Tauc et al. [22] in the case of germanium. Although this relation, valid near the absorption edge for $E > E_{\text{BG}}$, is based on several approximations, it fits our data in the energy range between 1.5 and 4 eV and it was also used in other works on amorphous carbon [18,23]. Thus the region where large clusters are predominant shows that the energy gap is larger than zero and smaller than 0.15 eV, while we find the RSC region characterized by an energy gap of 0.83 ± 0.3 eV. This is shown in panel (c) of Fig. 5. The loss of the semimetallic character in the region of small clusters has been attributed to the localization of the π -electrons [24]. Our measurements are in qualitative agreement with the results obtained from the characterization of nanostructured samples with ellipsometric techniques [25].

Our data indicate that XPS is not sensitive to the spatial distribution of the inhomogeneities in the NS samples at variance with Raman and EELS, which show spectral signatures of the predominant precursor clusters. In our samples a mixture of various chemical environments local to the carbon site is always present.¹ The density of states, as probed by XPS, is thus expected to average over a variety of spectral contributions representative of these carbon site inhomogeneities. Even though different weights of these specific components are expected to vary from sample to sample, it is likely that the overall DOS is not significantly affected.

In contrast, EELS is much more specific in its spectral response since it sees primarily how many “delocalized electrons” are present in the different specimen regions with respect to valence band electron bound into more localized configurations as might be the case of five-fold or seven-fold rings.

4. Conclusions

In this work we have analyzed nanostructured carbon thin films deposited with clusters of different size produced in

¹ C 1s XPS data, not shown here for space limitations, confirm the presence of this mixture.

supersonic beams. Raman spectroscopy shows that films with different nanostructures can be deposited by using different precursors. On the other hand, the XPS valence band spectra are not affected by structural difference of different film regions. To the best of our knowledge, the valence band shows a peak never observed in carbon thin films, which deserves novel theoretical calculations for further spectral assignment.

EELS shows important differences in the electronic structure between the region rich of small clusters and the region rich of large clusters. EELS data indicate that the precursors used to grow the film influence the electronic properties in terms of gap formation and density of delocalized electrons. Our investigation suggests that a delicate interplay exists between the structure and the electronic properties of cluster-assembled carbon. In order to elucidate the role played by different building blocks in influencing this interplay characterization of NS films grown in situ are currently underway.

Acknowledgements

This work was funded within the Progetto Ricerca Avanzata CLASS of the INFM and the MADESS-II project of the CNR. We thank L. Diederich, C. Lenardi, C.E. Bottani, and A. Li Bassi for many clarifying discussions. We are indebted with E. Maillard-Schaller and L. Schlapbach for providing us the diamond specimen.

References

- [1] L. Diederich, E. Barborini, P. Piseri, A. Podestá, P. Milani, A. Schneuwly, R. Gallay, *Appl. Phys. Lett.* 75 (1999) 2662.
- [2] R.H. Baughman, et al., *Science* 284 (1999) 1340.
- [3] A.C. Ferrari, B.S. Satyanarayana, J. Robertson, W.I. Milne, E. Barborini, P. Piseri, P. Milani, *Europhys. Lett.* 46 (1999) 245.
- [4] A. Perez, P. Melinon, V. Dupuis, P. Jensen, J. Tuaille, L. Bardotti, C. Martet, M. Treilleux, M. Pellarin, J.L. Vialle, B. Palpant, J. Lerme, *J. Phys. D: Appl. Phys.* 30 (1997) 709.
- [5] E. Barborini, P. Piseri, A. Li Bassi, A.C. Ferrari, C.E. Bottani, P. Milani, *Chem. Phys. Lett.* 300 (1999) 633.
- [6] P. Milani, S. Iannotta, *Cluster Beam Synthesis of Nanostructured Materials*, Springer, Berlin, 1999.
- [7] D. Donadio, L. Colombo, P. Milani, G. Benedek, *Phys. Rev. Lett.* 83 (1999) 776.
- [8] C.E. Bottani, A.C. Ferrari, A. Li Bassi, P. Milani, P. Piseri, *Europhys. Lett.* 42 (1998) 431.
- [9] E. Barborini, P. Piseri, P. Milani, *J. Phys. D: Appl. Phys.* 32 (1999) L105.
- [10] F. Sette, G.K. Wertheim, Y. Ma, G. Meigs, S. Modesti, C.T. Chen, *Phys. Rev. B* 41 (1990) 9766.
- [11] G. Comelli, J. Stohr, C.J. Robinson, W. Jark, *Phys. Rev. B* 38 (1988) 7511.
- [12] J. Robertson, *Prog. Solid State Chem.* 21 (1991) 199.
- [13] J. Schäfer, J. Ristein, R. Graupner, L. Ley, U. Stephan, Th. Frauenheim, V.S. Veerasamy, G.A.J. Amaratunga, M. Weiler, H. Ehrhardt, *Phys. Rev. B* 53 (1996) 7762.
- [14] U. Gelius, in: D.A. Shirley (Ed.), *Electron Spectroscopy*, North-Holland, Amsterdam, 1972, p. 311.
- [15] E. Schaller, *Diploma Thesis, Universite de Fribourg, Perolles, Switzerland, May 1992.*
- [16] F.R. McFeely, S.P. Kowalczyk, L. Ley, R.G. Cavell, R.A. Pollak, D.A. Shirley, *Phys. Rev. B* 9 (1974) 5268.
- [17] J.J. Yeh, I. Lindau, *Atomic Data and Nuclear Tables* 32 (1) (1985) 1–155.
- [18] P. Kovarik, E.B.D. Bourdon, R.H. Prince, *Phys. Rev. B* 48 (1993) 12 123.
- [19] F. Wooten, *Optical Properties of Solids*, Academic Press, New York, 1972.
- [20] R.F. Egerton, *Electron Energy-Loss Spectroscopy in the Electron Microscope*, Plenum, New York, 1986.
- [21] E.A. Taft, H.R. Phillipp, *Phys. Rev. A* 138 (1965) 197.
- [22] J. Tauc, R. Grigorovici, A. Vancu, *Phys. Stat. Sol.* 15 (1966) 627.
- [23] J. Fink, Th. Muller-Heinzerling, J. Pfluger, B. Scheerer, B. Dishler, P. Koidl, A. Bubenzer, R.E. Sha, *Phys. Rev. B* 30 (1984) 4713.
- [24] M.A. Tamor, C.H. Wu, *J. Appl. Phys.* 67 (1990) 1007.
- [25] P. Milani, M. Ferretti, P. Piseri, C.E. Bottani, A. Ferrari, A. Li Bassi, G. Guizzetti, M. Patrini, *J. Appl. Phys.* 82 (1997) 5793.